Molecular and Thermodynamic Basis for EGCG-Keratin Interaction-Part I: Molecular Dynamics Simulations

Jan K. Marzinek and Guoping Lian
Unilever Discover, Unilever R&D, Colworth, Sharnbrook, Bedfordshire MK44 1LQ, U.K.

Jan K. Marzinek, Athanasios Mantalaris, and Efstratios N. Pistikopoulos
Dept. of Chemical Engineering, Centre for Process Systems Engineering (CPSE), Imperial College London, London SW7 2BY, U.K.

Yanyan Zhao, Lujia Han, and and Longjian Chen
College of Engineering, China Agricultural University, Beijing 100083, P. R. China

Peter J. Bond
Dept. of Chemistry, The Unilever Centre for Molecular Science Informatics, University of Cambridge, Lensfield Road, Cambridge CB2 1EW, U.K.

Massimo G. Noro
Physical and Chemical Insights Group, Unilever R&D, Port Sunlight, Wirral CH63 3JW, U.K.

DOI 10.1002/aic.14220
Published online September 6, 2013 in Wiley Online Library (wileyonlinelibrary.com)

Nonspecific binding of small molecules to proteins influences transdermal permeation and intestinal absorption, yet understanding of the molecular and thermodynamic basis is still limited. In this study, we report all-atom, fully solvated molecular dynamics simulations of the thermodynamic characteristics of epigallocatechin-3-gallate (EGCG) binding keratin. Experimental validation is reported in Part II. Herein, 18 μs of simulation sampling was calculated. We show that the binding process is a combination of hydrophobic interaction, hydrogen bonding and aromatic interaction. The umbrella sampling technique was used to calculate the binding free energy of EGCG with keratin segments. By extracting EGCG from the keratin-EGCG complex using steered molecular dynamics, the rupture force was observed to be linearly related to the binding free energy. Multilayer binding of EGCG clusters to keratin has been shown. The binding free energy of -6.2 kcal mol^{-1} obtained from the simulations was in excellent agreement with the experimental Part II. © 2013 American Institute of Chemical Engineers *AIChE J*, 59: 4816–4823, 2013

Keywords: molecular dynamics, keratin, epigallocatechin-3-gallate, free energy, isothermal titration calorimetry

Introduction

Binding of small molecules to macromolecules of human biosubstrates regulates their subcellular disposition. The subject is fundamental to intestinal absorption of nutrients and drugs as well as transdermal permeation of cosmetic actives.[1,2] For example, there is an increasing interest in understanding the binding of plant actives, such as green tea with a high content of polyphenols, to human skin and intestinal proteins due to many health benefits.[3] A number of studies have been reported on the binding properties of polyphenols to milk and salivary proteins, using various experimental techniques.[4–7] Studies on the binding properties of human biosubstsrate proteins are still limited.

Epigallocatechin-3-gallate (EGCG), a natural antioxidant[8] and the main active polyphenol compound of green tea has been shown to have many benefits to human skin. These properties involve wound healing,[9] prevention of skin cancer,[10] antiaging,[8] as well as photoprotection[11,12] and immunomodulation.[13–16] The transdermal permeation is an important route[17] for delivering those small active molecules to the lower skin layers. The biological activity of green tea catechins mainly depends upon their bioavailability.[12,18] However, stratum corneum (SC), the outermost skin layer of the epidermis, constitutes the first barrier for skin permeation in which keratin constitutes the major component (80% of its dry mass[19]). Thus, the strength of the SC keratin-EGCG interaction regulates its bioavailability to the deeper skin layers and hence the delivery of vital profits.

Skin keratin is a typical epithelia intermediate filament (IF) protein with a very high degree of molecular diversity.

Additional Supporting Information may be found in the online version of this article.

Correspondence concerning this article should be addressed to G. Lian, at e-mail: guoping.lian@unilever.com

This article had been nominated by AIChE Session Chair, Dr. Jonathan Moore (Dow Chemical Company), as the "Best Presentation" at that session during the AIChE Annual Meeting in Pittsburgh, PA, Oct. 28–Nov. 2, 2012.

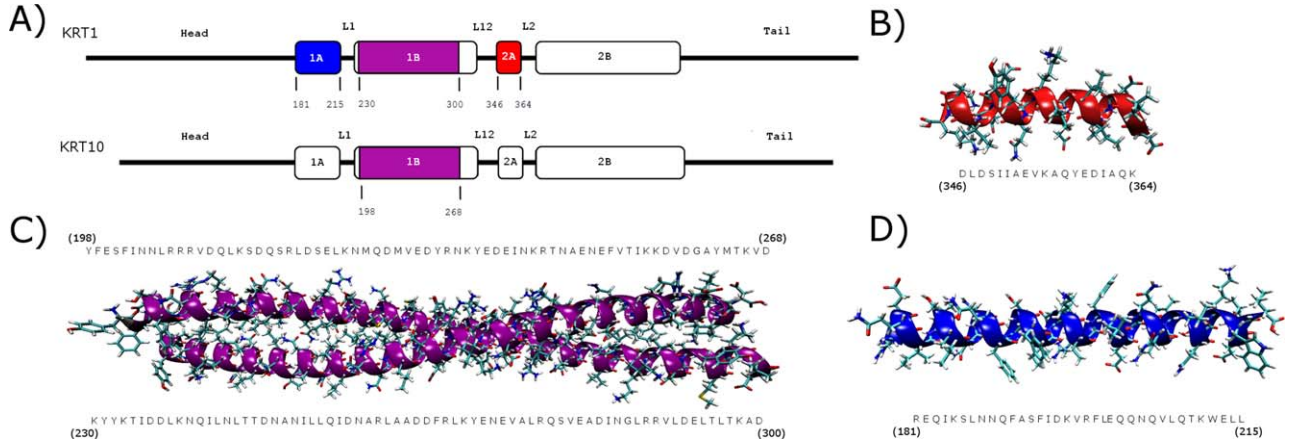

Figure 1. Segments and the corresponding sequence of keratin 1 and 10 used for MD simulations: (A) Schematic representation of chosen segments 1A (blue), 1B (purple), and 2A (red); (B) Helical segment 2A of keratin 1; (C) Coiled-coil 1B segment of keratin 1/ keratin 10; (D) Helical segment 1A of keratin 1.

[Color figure can be viewed in the online issue, which is available at wileyonlinelibrary.com.]

These heteropolymeric filaments are built by pairing acidic (type I) and basic (type II) molecules forming a dynamic network of 10–12 nm in size.[20] All keratins possess a tripartite domain structure which is characteristic to IFs. The central α-helical domain (rod) is a major determinant of self-assembly. At the N- and C-termini are nonhelical "head" and "tail" domains. Monomeric keratin consists of α-helical segments 1A, 1B, 2A, 2B. Two monomeric units form a parallel left-handed coiled-coil dimer in which each α-helical chain has a characteristic sequence of heptad motif, (abcdefg), which repeats along the chain.[21] The residues "a" and "d" are known to be occupied by nonpolar amino acids, building up a hydrophobic strand between α-helices. Residues "e" and "g" have opposing charges and attract each other by electrostatic interactions forming a salt bridge. Residues "b," "c," and "f" are hydrophilic. Two assembled coiled-coils form a tetramer. Further aggregation of tetramers leads to the formation of protofilaments. Right-handed, rope-like structures of protofibrils are the final conformations of IFs. The most abundant pair in the upper epidermis and SC forming IFs is keratin type 1 and 10, and constitutes the subject of this study.[22]

Molecular dynamics (MD) simulations are used here to study EGCG-keratin interactions. The simulation approach provides detailed information at the atomic level which cannot be observed by experiment alone. Self-assembly simulations totalling ~6 μs were first used to generate possible keratin-EGCG bound states at a range of concentrations and temperatures. In addition, steered constant-velocity molecular dynamics (SMD) simulations were used to pull EGCG molecules away from the keratin surface. In SMD, a constant force or velocity is applied to the center of mass (COM) of a specified group of atoms attached to a "virtual spring." In this way, SMD provides information about structural changes and mechanical properties of proteins or protein-ligand complexes.[23] The rupture force (the breaking point) can provide information about the strength of the interaction. During the SMD simulations presented herein, the force was observed to reach a maximum point when stabilizing hydrogen bonds were broken between keratin and EGCG. Subsequently, snapshots from the SMD simulations provided starting points for the umbrella sampling (US) method.[24,25] US is a biased MD approach in which an additional harmonic potential ensures sufficient sampling along a defined reaction coordinate over multiple overlapping simulations (windows), enabling calculation of the potential of mean force (PMF).[26] US has previously been applied successfully to a wide range of systems, yielding good thermodynamic agreement with experimental data in many cases.[27–30] Herein, we used ~12 μs of US in order to calculate the free energy of binding of EGCG to keratin at different temperatures.

Previously, Zhao et al.[31] showed that EGCG binds to gastric mucin by a combination of hydrophobic interactions and hydrogen bonding. Multilayer binding of polyphenol was suggested, and a decrease in binding affinity with increasing temperature was observed. In Part II, of this study, the thermodynamic properties of keratin-EGCG interactions have been quantitatively determined using ultrafiltration, high-performance liquid chromatography (HPLC), and isothermal titration calorimetry (ITC). The multilayer isotherm has been reported and hence the experimental investigation supports MD simulations where EGCG clusters to keratin forming a multilayer assembly. In addition, the binding energies predicted from MD simulations are in excellent agreement with the ITC data.

Methodology

Computational details

The structure of EGCG was built using Chimera 1.5.3.[32] To create the EGCG topology the CHARMM general force field (CGenFF)[33–36] for organic molecules (program version 0.9.1 beta) was used and translated into GROMACS topology format using in-house code. A coiled-coil keratin fragment was modeled based on the Cortexillin I domain (Protein Data Bank entry: 1D7M). The cortexillin and keratin 1/keratin 10 residues heptad repeats (abcdefg) were predicted using Matcher (algorithm for matching coiled-coil proteins).[37] Each helical fragment of the cortexillin coiled coil consists of 101 residues, of which 71 residues corresponding to segment 1B of keratin type 1 and 10 were chosen. Predicted cortexillin repeats were mutated into the keratin sequences. Alpha helical segment 1A (35 residues)

Table 1. Details of Self-Assembly Simulations for Keratin-EGCG Interactions.

System No.	Segment	Number of EGCG molecules	Simulation time (ns)	Temperature (K)	Number of simulations
1.	1A	1	100	298	5
2.	1A	1	100	308	5
3.	1A	1	100	318	5
4.	2A	1	100	298	4
5.	2A	1	100	308	4
6.	2A	1	100	318	4
7.	1B	1	100	298	8
8.	1B	1	100	308	8
9.	1B	1	100	318	8
10.	1B	20	200	298	3

and 2A (19 residues) of keratin 1 were built using Chimera. The amino acid sequences of all keratin segments were taken from the Human IF Database.[38] Initial structures were minimized via the steepest descent (SD) algorithm. The chosen segments, constructed models, and corresponding sequences are presented in Figure 1.

All MD and SMD simulations were performed using the GROMACS 4.5.4[39] package with the CHARMM22/CMAP[40] force field and the TIP3P[41] water model. Classical equations of motion were integrated with a Verlet leap-frog algorithm using a 2-fs time step. The LINCS[42] algorithm was used to constrain bond lengths. A 1.4-nm cutoff distance was used for the short-range neighbor list, updated every five steps (10 fs), and van der Waals interactions were cutoff at 1.4 nm. The particle mesh Ewald method[43,44] was used for the electrostatics with a 1.2-nm real space cutoff. The velocity rescale thermostat and Parinello–Rahman[45] barostat were used to maintain the temperature and pressure (at 1 bar), respectively. Protein or protein and ligand were coupled to one bath, while the remaining water and ions were coupled to the other. The initial velocities were set to follow a Maxwell distribution. Periodic boundary conditions were used in all directions. All simulations were run on the two Linux clusters (Department of Chemical Engineering Computing Service: imperial.ac.uk/chemicalengineering and Imperial College High Performance Computing Service: imperial.ac.uk/ict/services/teachingandresearchservices/highperformancecomputing, Imperial College London).

Self-assembly simulation setup

Different keratin segments were placed at the center of a cubic unit cell: Segment 1B (12 × 12 × 12 nm), segment 1A (8 × 8 × 8 nm), and segment 2A (6 × 6 × 6 nm). To mimic the fact that both the helix and coiled-coil segments are part of the IF, terminal residues were treated in their uncharged state.

Initially, one EGCG molecule was placed into the box in a random position near to the given keratin segment. Each system involved one keratin segment (1A, 2A, or 1B) and one EGCG molecule. The simulation box was filled with water using the TIP3P water model, to which 150 mM NaCl was added to neutralize the system charge. Following energy minimization using the SD algorithm, 200 ps of sequential NVT (constant number of atoms N, constant volume V, constant temperature T) and NPT (constant number of atoms N, constant pressure P, constant temperature T) equilibration simulations were conducted, with position restraints applied to protein and ligand heavy atoms. Production simulations were then performed in the NPT ensemble at 298, 308, and 318 K.

In total, 51 EGCG-keratin MD simulations of 100 ns were run with one EGCG molecule placed at different initial positions around given keratin segment. This involved, in each case for three different temperatures: eight simulations with coiled-coil segment 1B, five simulations with helical segment 1A, and four simulations with helical segment 2A. The number of simulations corresponds to the size of the given protein segment and thus different possibilities to place EGCG randomly.

Following the same procedure in order to assess higher concentration of EGCG, three additional simulations of 200 ns at 298 K were performed with 20 EGCG molecules placed a minimum of 6 nm away from the coiled-coil fragment starting from different initial coordinates of EGCG molecules. Each system and corresponding self assembly simulation is listed in Table 1.

Biased simulation setup

The final coordinates of the keratin-EGCG complex from the self-assembly MD simulations were set as the initial configurations for SMD simulations. For each complex, the COM of an EGCG molecule was increased at a constant rate (velocity), being pulled up to 4 nm away, in a direction (reaction coordinate) perpendicular to the protein backbone axis. As the simulation proceeded the pulling force was observed to increase, up to the point where the first keratin-EGCG hydrogen bond was broken. The breaking point of each hydrogen bond corresponds to a local maximum in the pulling force.

Steered MD was used to extract the initial coordinates for US windows (binding free energy calculations). A weighted histogram analysis method (WHAM)[46,47] was then applied to combine all windows into the PMF curve to estimate the binding free energy difference along the reaction coordinate (distance). The statistical error estimate of each PMF curve was performed using Bayesian bootstrapping.[48]

Analysis

The average number of hydrogen bonds between protein and EGCG was counted based on the cutoff distance between the donor and the acceptor atoms below 3.5 Å and a hydrogen-donor–acceptor maximum angle of 30°. The buried area between the protein and ligand was computed by subtracting solvent accessible surface area (SAS)[49] of the protein and EGCG from SAS of keratin-EGCG complex. Both hydrogen bonds and buried area were extracted from equilibrium simulations, prior to SMD simulations and US.

Results and Discussion

Monomeric self-assembly simulations

Simulated tea catechin (EGCG) molecule became attached to multiple (between 1 and 5) residues at the end of each

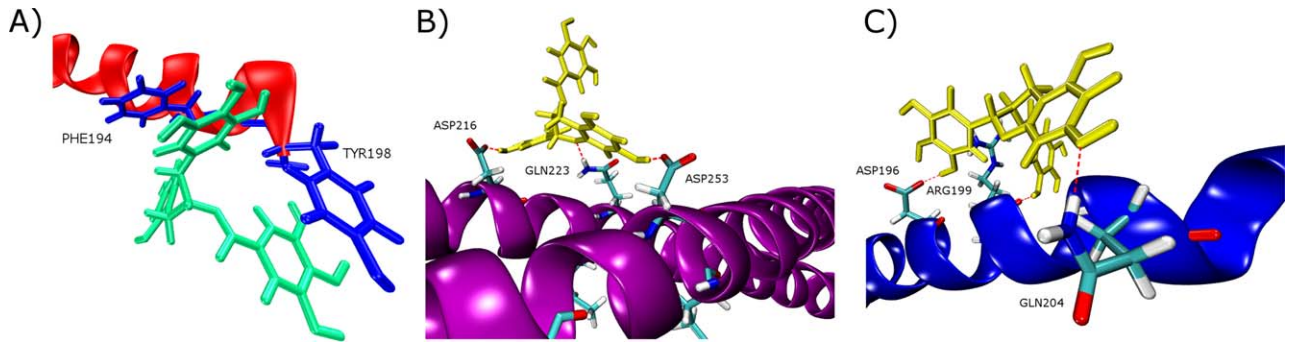

Figure 2. Final configurations of MD simulations: (A) Segment 1A (red) and its two aromatic residues (blue) stacked via aromatic attraction to two EGCG (green) rings; (B) Segment 1B coiled coil (purple) and EGCG (yellow) occupying three different residues via hydrogen bonds at 308 K; (C) Segment 1A (blue) and EGCG (yellow) occupying three different residues via hydrogen bonds (red dotted lines) at 298 K.

[Color figure can be viewed in the online issue, which is available at wileyonlinelibrary.com.]

simulation replica in the system for a single EGCG and one keratin segment (Table 1–Simulation no. 1–9). An example of the Keratin-EGCG hydrophobic buried area as well as the number of hydrogen bonds vs. simulation time is presented in Supporting Information, Figure S1. Hydrophobic interactions played a major role in the initial stages of protein-ligand assembly, followed by a slow optimization via formation of hydrogen bonds. In many cases, stacking interactions were observed in which the aromatic rings of EGCG became packed against those of phenylalanine or tyrosine (Figure 2A). Side chains of acidic residues were predominantly occupied by catechin, supported by the fact that EGCG contains 8 hydrogen donors and 11 hydrogen acceptors (Figures 2B, C). This confirms previous investigations in which EGCG was shown to interact specifically with charged amino acids.[50] In this study, once an acidic side chain oxygen or nitrogen had created a hydrogen bond with the EGCG hydroxyl group, it was subsequently persistent for the remaining simulation time (Figures 2A, B). In Supporting Information, Table T1, the occupied keratin residues, as well as the average number of hydrogen bonds formed between EGCG and acidic residues of the coiled-coil segment 1B, during 100 ns of simulation at 298 K are presented. The binding contribution of acidic amino acids varies widely from ~30 to 100% due to the exposed hydrogen bond acceptors of their side chains, interacting with the multiple EGCG hydroxyl groups. At 318 K, in 3 out of 17 self-assembly monomeric EGCG-keratin simulations (each of 100 ns), the EGCG molecule stacked onto the keratin surface after ~2–5 ns, and remained attached for ~40–60 ns before detaching, suggesting weaker interactions at higher temperatures (Supporting Information, Figure S2. Keratin-EGCG total buried area vs. the simulation time). In contrast, at 298 and 308 K, EGCG always remained bound to the keratin surface.

Multilayer self-assembly

In the simulation of 20 EGCG molecules and keratin coiled fragment (Table 1–Simulation no. 10), EGCG molecules tended to bind to keratin as clusters. Snapshots from this simulation over the 200 ns are presented in Figure 3. Initially, individual EGCG molecules were placed 6 nm away from coiled-coil part and away from each other. After 1 ns, EGCG started to aggregate into small clusters (2–3 EGCG), and further clustering was observed by 10 ns (~2–7 molecules) driven primarily by hydrophobic attraction. Within the next 30 ns, three clusters of 6–7 EGCG were formed and one adsorbed onto the protein surface. By 100 ns, two large EGCG aggregates were bound to the keratin surface, with one remaining in the bulk. After 120 ns, a cluster of all 20 molecules were attached to the coiled coil, and gradually spread over the protein surface. The snapshot at 200 ns (Figure 3) shows an elongated EGCG cluster adsorbed onto the protein as multilayer. In Supporting Information, Figure S3 the number of hydrogen bonds between EGCG molecules only and keratin-EGCG over the course of the simulation is presented. It may be observed that EGCG molecules bind to each other within first 2 ns via hydrogen bonds forming small clusters by further formation of big aggregates. The number of hydrogen bonds between EGCG molecules and the coiled-coil part of keratin shows an

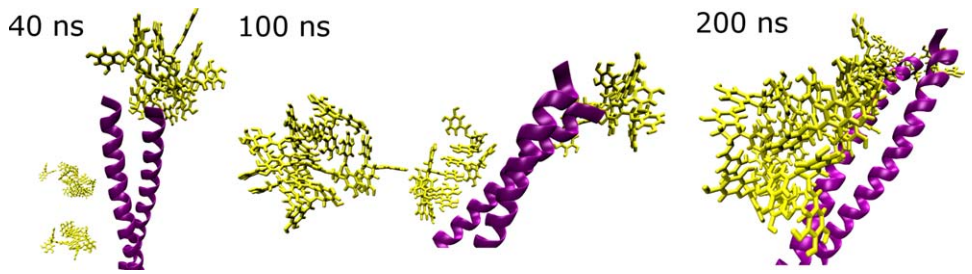

Figure 3. Conformations throughout the simulation of keratin coiled-coil segment (purple) and 20 EGCG molecules (yellow) at 298 K.

The formation of clusters is observed by further spreading EGCG molecules over the keratin surface as multilayer. [Color figure can be viewed in the online issue, which is available at wileyonlinelibrary.com.]

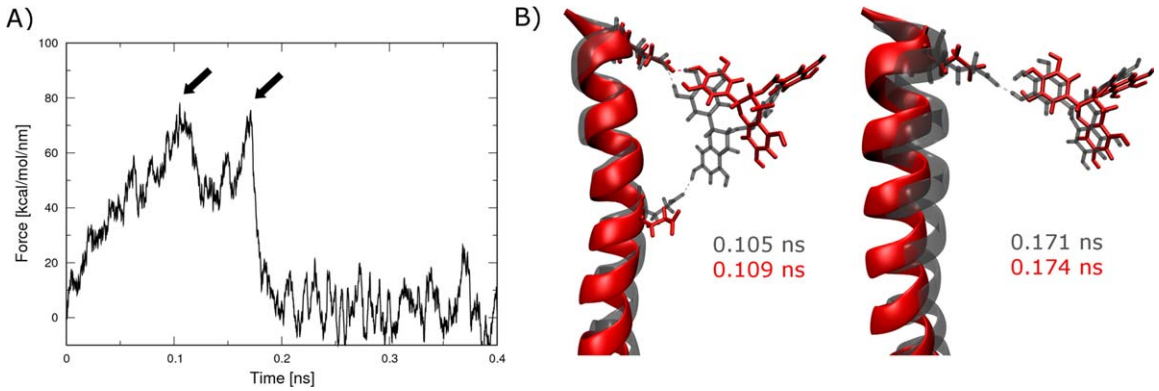

Figure 4. An example of SMD simulation in EGCG-keratin complex: (A) Pulling force vs. time–two breaking maxima correspond to hydrogen bond breakage at 0.105 and 0.171 ns; (B) Snapshots from SMD simulation corresponding to the first and second maximum pulling force, respectively.

[Color figure can be viewed in the online issue, which is available at wileyonlinelibrary.com.]

increasing number due to the elongation on the keratin surface which is confirmed by covering the EGCG hydrophobic area (Supporting Information, Figure S4). As nearly 50% of SC keratin residues are nonpolar, the hydrophobic collapse followed by hydrogen bonding optimization represented the primary mechanism for EGCG aggregation and binding to keratin. We can, therefore, confirm that the formation of EGCG multilayer is in agreement with previous investigations of ultrafiltration and HPLC experiments in mucin-EGCG system.[31]

Assessment of biased MD simulation protocol

An example of SMD simulation is shown in Figure 4. The first force maximum was reached at 0.105 ns corresponding to the breakage of the first hydrogen bond with a value of 77 kcal mol^{-1} nm^{-1}. The second maximum of the pulling force was at 0.171 ns with a value of 75 kcal mol^{-1} nm^{-1}. For such SMD trajectories, the breaking point of the complex is defined as the highest value of the reached force.

As the initial coordinates for US windows were obtained from SMD simulations, the effect of pulling rate and virtual spring constant in SMD on the binding free energy was assessed. EGCG was pulled away from segment 1A at 298 K for 0.4 ns at 10 nm ns^{-1} and for 4 ns at 1 nm ns^{-1} using harmonic spring constants of 120 kcal mol^{-1} nm^{-2} and 360 kcal mol^{-1} nm^{-2}, respectively. By using the spacing of approximately 0.2 nm along the reaction coordinate (distance) for both SMD simulations, the initial configurations for US windows were extracted. Subsequently, 20 US window simulations of 50 ns each were calculated using a harmonic biased potential for both cases, with a spring constant of 120 kcal mol^{-1} nm^{-2}. The WHAM method was then applied to obtain the final PMF curve neglecting the first 3 ns of each window for the system equilibration. With both different pulling rates and spring constants nearly the same values (0.15 kcal mol^{-1} difference) of binding free energy difference were achieved. The corresponding plots of force vs. time and PMF profiles can be found in the Supporting Information, Figure S5–S7.

Hence, the fast pulling rate of 10 nm ns^{-1} was used in all subsequent keratin-EGCG SMD simulation systems, with a spring constant of 120 kcal mol^{-1} nm^{-2}. The corresponding methodology for calculating the binding free energy difference (0.2 nm spaced 50 ns simulations with harmonic spring constant of 120 kcal mol^{-1} nm^{-2}) was applied. An example of the convergence of the PMF is presented in Supporting Information, Figure S8 along with US histograms showing excellent overlap (Supporting Information, Figure S9).

To confirm the reproducibility of fast pulling for each system, SMD was performed three times with the same pulling conditions. An example of SMD simulation (force vs. time) for removing EGCG from the keratin coiled-coil fragment at 308 K from the same initial coordinates is presented in the Supporting Information, Figure S10. Nearly identical trajectories were produced with approximately the same rupture force (maximum pulling force).

Steered MD and US

The free energy calculations were performed based on the results from monomeric (one EGCG molecule and given keratin segment) self-assembly simulations. From all 17 self-assembly simulations at 298 and 308 K, we extracted the final coordinates of the EGCG-keratin complex and ran 17 SMD simulations at given temperature to pull the EGCG away from the keratin surface. As at 318 K in three cases EGCG spontaneously detached, we followed the same procedure with 14 self-assembly results. For a given temperature, we compared all maximum pulling forces (breaking points) and chose the ones with the highest, lowest and median values of the maximum force. Those SMD trajectories were used to extract the initial coordinates for free energy calculations. We used five SMD trajectories for 298 K, three for 308 K, and three for 318 K. In Figure 5, results from SMD simulations and US are presented. The force vs. time profiles and corresponding PMF curves (the same colours) can be observed for a given temperature. The energy minima of PMF curves correspond to the initial coordinates at which EGCG was adsorbed to the keratin surface. As the distance between those two groups increased the PMF increased, eventually reaching a plateau between 1–2 nm in all cases.

The correlation between the average number of hydrogen bonds and buried EGCG/keratin surface area vs. binding free energy is presented in Figure 6. The free energy (ΔG) value of -5.3 kcal mol^{-1} was obtained from one simulation at 298 K where EGCG stacking interactions (Figure 2A) with tyrosine/phenylalanine residues were dominant providing only 0.87 of the average number of hydrogen bonds. This data point on the plot (Figure 6A) was, therefore, omitted as

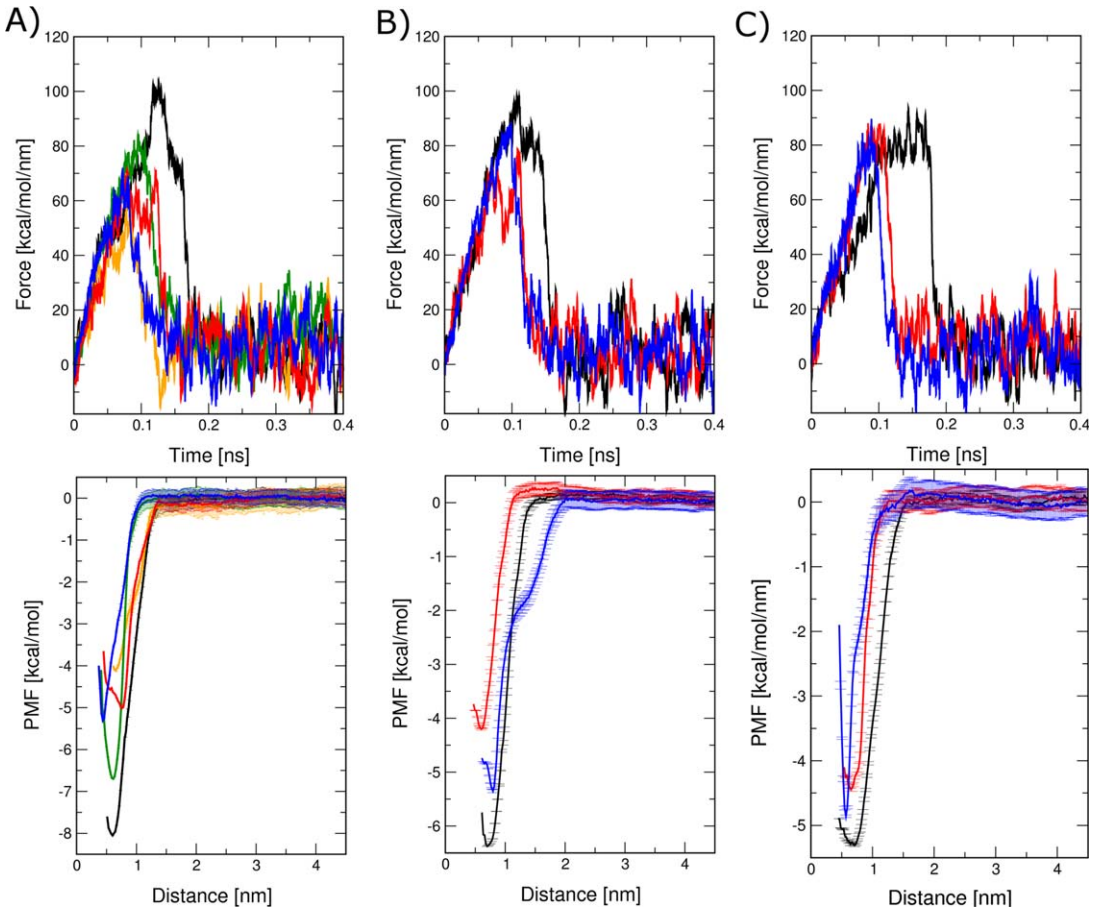

Figure 5. Force vs. time profiles of pulling EGCG away from different keratin segments (1B-black and green; 1A-red and orange, 2A-blue) and corresponding PMF curves at: (A) 298 K; (B) 308 K; (C) 318 K.

[Color figure can be viewed in the online issue, which is available at wileyonlinelibrary.com.]

hydrogen bonding was not the main interaction. The free energy "distance" of this point from the linear correlation suggests that the aromatic attraction would account for approximately 2–3 kcal mol^{-1} of the binding free energy for this system. Therefore, aromatic interactions play a significant role in initial stabilization/assembly due to the approximately 10% content of aromatic residues in SC keratin type 1 and 10. Thus, there is a strong linear correlation of the average number of hydrogen bonds between EGCG with nonaromatic keratin residues.

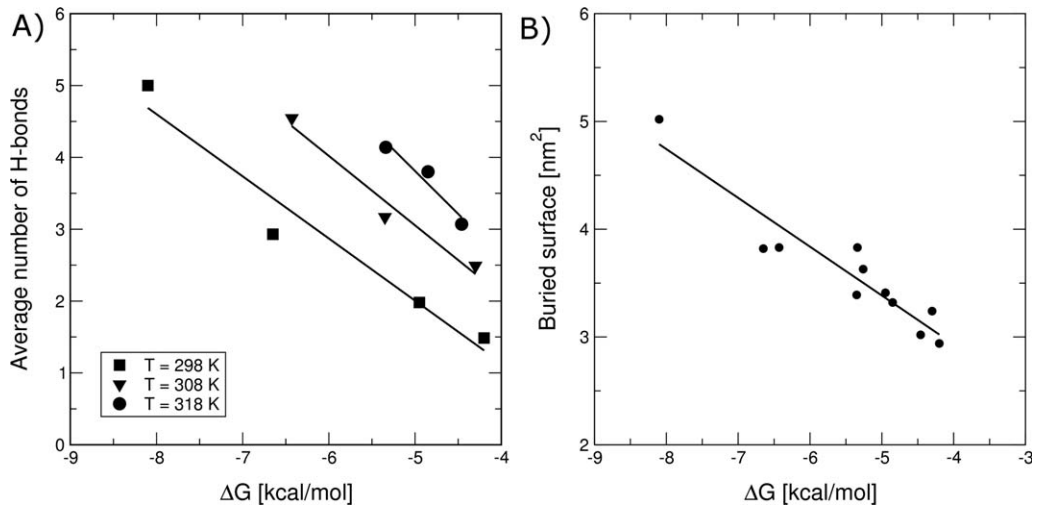

Figure 6. (A) The average number of hydrogen bonds between EGCG and keratin vs. the binding free energy difference (at 298 K: $R^2 = 0.97$, at 308 K: $R^2 = 0.98$, at 318 K: $R^2 = 0.96$)–the point corresponding to $\Delta G = -5.3$ kcal mol^{-1} and 0.87 of the average number of hydrogen bonds due to the aromatic attraction governed process was omitted; (B) EGCG/keratin buried surface area (determined from the NPT equilibration prior pulling simulations) with respect to the binding free energy difference ($R^2 = 0.94$).

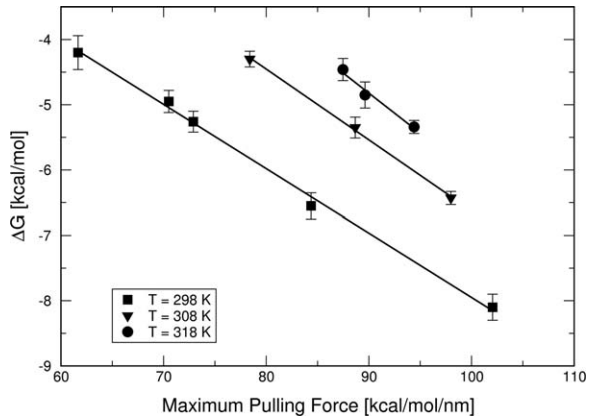

Figure 7. The linear correlations between the maximum pulling force (each value obtained from 0.4 ns of SMD simulations) and the free energy obtained by US (each point corresponds to 1 μs of sampling) calculations ($R^2 = 0.99$ in all cases).

Figure 6 also shows that the higher the value of the buried surface area between EGCG and keratin, the greater the magnitude of ΔG, at all three temperatures. In all cases, EGCG expelled water molecules from the keratin surface and became directly bound to the keratin during adsorption, suggesting the potential for a favorable entropic contribution to the binding process. An example of decreasing number of hydrogen bonds between EGCG and water over the binding process to keratin is presented in Supporting Information, Figure S11.

As described above, from each SMD simulation, the maximum pulling force may be obtained. A linear correlation of the rupture force (obtained in all cases at the same pulling rate) vs. the free energy ΔG of binding is observed in Figure 7. With a single pulling SMD simulation for 0.4 ns, it is possible to estimate the binding affinity in this system instead of time consuming US calculations (1 μs). The implication is that based on the strong linear correlation it may be possible to estimate the free energy for other small molecules binding the most common α-helical motif via hydrogen bonds and/or hydrophobic collapse using single SMD simulation.

The binding free energy at a given temperature was estimated on the basis of the maximum and minimum observed ΔG values, corresponding to $\Delta G_{298} = -6.2$ kcal mol^{-1}, $\Delta G_{308} = -5.4$ kcal mol^{-1}, and $\Delta G_{318} = -4.9$ kcal mol^{-1}, respectively. The binding affinity decreases as temperature increases due to the increase in the kinetic energy (mobility) of molecules, hence leading to weaker interactions.

Conclusions

EGCG, the main active green tea polyphenol is used as an additive in skin care applications because of its antioxidant, photoprotective, immunomodulatory, and antiaging properties. The biological activity of EGCG mainly depends upon its bioavailability. SC constitutes the first barrier for transdermal permeation of active molecules. Due to the high content of keratin in SC (80% of its dry mass) the strength of the keratin-EGCG interaction regulates its bioavailability in the deeper skin layers. An understanding of those molecular interactions of the most active green tea polyphenol (EGCG) with skin protein requires characterization of the thermodynamic properties of the system as well as atomic-scale structure and dynamics.

For the first time, it has been shown that EGCG binds to the helical and coiled-coil part of type I and II human keratin IF expressed in the SC. MD simulations of various keratin-EGCG interaction systems have been performed for a total of 18 μs starting from different initial configurations at three different temperatures. Computer simulations revealed that hydrophobic assembly and in many cases aromatic interactions followed by hydrogen bonding are the key mechanisms governing the binding of EGCG to keratin. The significance of the interactions with acidic amino acid side chains with EGCG has been also shown. The previously suggested[31] multilayer binding of EGCG to mucin via both hydrogen bonds and hydrophobic collapse is confirmed to be responsible for binding in the EGCG-keratin system at higher concentrations. In those simulations, EGCG molecules formed clusters which bind to keratin and spread over its surface. The increase in temperature results in a decrease in the EGCG binding affinity toward keratin and the average number of hydrogen bonds between them. At constant temperature the breaking point (rupture force) from short SMD simulations and the binding free energy difference from time consuming US simulations were shown to be linearly correlated. This indicates that it should be possible to make good estimates of the binding free energy for other small molecules to the keratin surface from SMD simulations alone.

In Part II, the experimental results are presented. The multilayer isotherm based on ultrafiltration and HPLC has been reported, supporting the above MD simulations results. In addition, the binding free energy obtained from the MD simulation ($\Delta G = -6.20$ kcal mol^{-1}) is in excellent agreement with the ITC experimental data ($\Delta G = -6.37$ kcal mol^{-1}).

Acknowledgments

This contribution was identified by Jonathan Moore (The Dow Chemical Company) as the Best Presentation in the session "Industrial Applications of Computational Chemistry and Molecular Simulation III" of the 2012 AIChE Annual Meeting in Pittsburgh, PA. The research leading to these results has received funding from the EC's Seventh Framework Programme [FP7/2007–2013] under Grant Agreement N° 238013 which is greatly acknowledged. The first author wishes to thank Dr. Robert Farr and Dr. Anna Akinshina for providing stimulating discussions. Longjian Chen wishes to thank National Natural Science Foundation of China for the funding (Project No. 21006124).

Literature Cited

1. Hansen S, Selzer D, Schaefer UF, Kasting GB. An extended database of keratin binding. *J Pharm Sci*. 2011;100:1712–1726.
2. Wang LM, Chen LJ, Lian GP, Han LJ. Determination of partition and binding properties of solutes to stratum corneum. *Int J Pharm*. 2010;398:114–122.
3. Singh BN, Shankar S, Srivastava RK. Green tea catechin, epigallocatechin-3-gallate (EGCG): mechanisms, perspectives and clinical applications. *Biochem Pharmacol*. 2011;82:1807–1821.
4. Bennick A. Interaction of plant polyphenols with salivary proteins. *Crit Rev Oral Biol Med*. 2002;13:184–196.
5. Charlton AJ, Baxter NJ, Lilley TH, Haslam E, McDonald CJ, Williamson MP. Tannin interactions with a full-length human salivary proline-rich protein display a stronger affinity than with single proline-rich repeats. *FEBS Lett*. 1996;382:289–292.
6. Charlton AJ, Baxter NJ, Khan ML, et al. Polyphenol/peptide binding and precipitation. *J Agric Food Chem*. 2002;50:1593–1601.
7. Siebert KJ, Troukhanova NV, Lynn PY. Nature of polyphenol-protein interactions. *J Agric Food Chem*. 1996;44:80–85.

8. Masaki H. Role of antioxidants in the skin: anti-aging effects. *J Dermatol Sci*. 2010;58:85–90.
9. Leu JG, Chen SA, Chen HM, et al. The effects of gold nanoparticles in wound healing with antioxidant epigallocatechin gallate and alpha-lipoic acid. *Nanomedicine*. 2012;8:767–775.
10. Yang CS, Lambert JD, Ju J, Lu G, Sang S. Tea and cancer prevention: molecular mechanisms and human relevance. *Toxicol Appl Pharmacol*. 2007;224:265–273.
11. Katiyar SK, Elmets CA. Green tea polyphenolic antioxidants and skin photoprotection (Review). *Int J Oncol*. 2001;18:1307–1313.
12. Heinrich U, Tronnier H, De Spirt S, Stahl W. Green tea polyphenols provide photoprotection and improve physiological parameters of human skin. *Agro Food Ind Hi Tech*. 2011;22:38–39.
13. Elmets CA, Singh D, Tubesing K, Matsui M, Katiyar S, Mukhtar H. Cutaneous photoprotection from ultraviolet injury by green tea polyphenols. *J Am Acad Dermatol*. 2001;44:425–432.
14. Katiyar S, Elmets CA, Katiyar SK. Green tea and skin cancer: photoimmunology, angiogenesis and DNA repair. *J Nutr Biochem*. 2007;18:287–296.
15. Katiyar SK. Green tea prevents non-melanoma skin cancer by enhancing DNA repair. *Arch Biochem Biophys*. 2011;508:152–158.
16. Record IR, Dreosti IE. Protection by black tea and green tea against UVB and UVA+B induced skin cancer in hairless mice. *Mutat Res*. 1998;422:191–199.
17. Pathan IB, Setty CM. Chemical penetration enhancers for transdermal drug delivery systems. *Trop J Pharm Res*. 2009;8:173–179.
18. Afaq F, Katiyar SK. Polyphenols: skin photoprotection and inhibition of photocarcinogenesis. *Mini Rev Med Chem*. 2011;11:1200–1215.
19. Williams AC, Barry BW. Skin absorption enhancers. *Crit Rev Ther Drug Carrier Syst*. 1992;9:305–353.
20. Norlen L, Al-Amoudi A. Stratum corneum keratin structure, function, and formation: the cubic rod-packing and membrane templating model. *J Invest Dermatol*. 2004;123:715–732.
21. Feughelman M. *Mechanical Properties and Strucutre of a-Keratin Fibres*. Sydney: University of New South Wales Press, 1997:119–121.
22. Norlen L. Stratum corneum keratin structure, function and formation – a comprehensive review. *Int J Cosmet Sci*. 2006;28:397–425.
23. Izrailev S, Stepaniants S, Schulten K. Applications of steered molecular dynamics to protein-ligand/membrane binding. *Biophys J*. 1998;74:A177.
24. Torrie GM, Valleau JP. Monte-carlo free-energy estimates using non-boltzmann sampling – application to subcritical lennard-jones fluid. *Chem Phys Lett*. 1974;28:578–581.
25. Torrie GM, Valleau JP. Non-physical sampling distributions in monte-carlo free-energy estimation – umbrella sampling. *J Comput Phys*. 1977;23:187–199.
26. Kastner J. Umbrella sampling. *Wiley Interdiscip Rev Comput Mol Sci*. 2011;1:932–942.
27. Woo HJ, Roux B. Calculation of absolute protein-ligand binding free energy from computer simulations. *Proc Natl Acad Sci USA*. 2005;102:6825–6830.
28. Feenstra P, Brunsteiner M, Khinast J. Prediction of drug-packaging interactions via molecular dynamics (MD) simulations. *Int J Pharm*. 2012;431:26–32.
29. Chen PC, Kuyucak S. Accurate determination of the binding free energy for kcsa-charybdotoxin complex from the potential of mean force calculations with restraints. *Biophys J*. 2011;100:2466–2474.
30. Buch I, Sadiq SK, De Fabritiis G. Optimized potential of mean force calculations for standard binding free energies. *J Chem Theory Comput*. 2011;7:1765–1772.
31. Zhao Y, Chen L, Yakubov G, Aminiafshar T, Han L, Lian G. Experimental and theoretical studies on the binding of epigallocatechin gallate to purified porcine gastric mucin. *J Phys Chem B*. 2012;116:13010–13016.
32. Pettersen EF, Goddard TD, Huang CC, Couch GS, Greenblatt DM, Meng EC, Ferrin TE. UCSF chimera - a visualization system for exploratory research and analysis. *J Comput Chem*. 2004;25:1605–1612.
33. Vanommeslaeghe K, Ghosh J, Polani NK. Sheetz M, Pamidighantam SV, Connolly JWD, MacKerell AD Jr. Automation of the charmm general force field for drug-like molecules. *Biophys J*. 2011;100:611.
34. Vanommeslaeghe K, Raman EP, MacKerell AD. Automation of the CHARMM general force field (CGenFF) II: assignment of bonded parameters and partial atomic charges. *J Chem Inf Model*. 2012;52:3155–3168.
35. Vanommeslaeghe K, Hatcher E, Acharya C, Kundu S, Zhong S, Shim J, Darian E, Guvench O, Lopes P, Vorobyov I, Mackerell AD Jr. CHARMM general force field: a force field for drug-like molecules compatible with the CHARMM all-atom additive biological force fields. *J Comput Chem*. 2010;31:671–690.
36. ParamChem Interface. Available at https://www.paramchem.org. Last Accessed 2013.
37. MATCHER - algorithm for matching coiled-coil proteins. Available at http://cis.poly.edu/~jps/. Last accessed 2012.
38. Szeverenyi I, Cassidy AJ, Chung CW, Lee BT, Common JE, Ogg SC, Chen H, Sim SY, Goh WL, Ng KW, Simpson JA, Chee LL, Eng GH, Li B, Lunny DP, Chuon D, Venkatesh A, Khoo KH, McLean WH, Lim YP, Lane EB. The human intermediate filament database: comprehensive information on a gene family involved in many human diseases. *J. Chem. Theory Comput*. 2008;4:435–447.
39. Hess B. GROMACS 4: algorithms for highly efficient, load-balanced, and scalable molecular simulation. *Abstr Pap Am Chem Soc*. 2009:237.
40. Bjelkmar P, Larsson P, Cuendet MA, Hess B, Lindahl E. Implementation of the CHARMM force field in GROMACS: analysis of protein stability effects from correction maps, virtual interaction sites, and water models. *J Comput Chem*. 2010;6:459–466.
41. Berendsen HJC, Postma JPM, van Gunsteren WF, Hermans J. *Intermolecular Forces*, Vol. B14. In: B. Pullman, editor. D. Reidel Publishing Company, 1981:331–342.
42. Hess B, Bekker H, Berendsen HJC, Fraaije JGEM. LINCS: a linear constraint solver for molecular simulations. *J Comput Chem*. 1997;18:1463–1472.
43. Darden T, York D, Pedersen L. Particle mesh ewald - an N.log(N) method for ewald sums in large systems. *J Chem Phys*. 1993;98:10089–10092.
44. Essmann U, Perera L, Berkowitz ML, Darden T, Lee H, Pedersen LG. A smooth particle mesh ewald method. *J Chem Phys*. 1995;103:8577–8593.
45. Parrinello M, Rahman A. Crystal structure and pair potentials: a molecular-dynamics study. *Phys Rev Lett*. 1980;45:1196–1199.
46. Kumar S, Bouzida D, Swendsen RH, Kollman PA, Rosenberg JM. The weighted histogram analysis method for free-energy calculations on biomolecules. *J Comput Chem*. 1992;13:1011–1021.
47. Hub JS, De Groot BL, Van Der Spoel D. g_wham-A free weighted histogram analysis implementation including robust error and autocorrelation estimates. *J Chem Theory Comput*. 2010;6:3713–3720.
48. Rubin DB. The bayesian bootstrap. *Ann Stat*. 1981;9:130–134.
49. Eisenhaber F, Lijnzaad P, Argos P, Sander C, Scharf M. The double cubic lattice method - efficient approaches to numerical-integration of surface-area and volume and to dot surface contouring of molecular assemblies. *J Comput Chem*. 1995;16:273–284.
50. Popovych N, Brender JR, Soong R, Vivekanandan S, Hartman K, Basrur V, Macdonald PM, Ramamoorthy A. Site specific interaction of the polyphenol EGCG with the SEVI amyloid precursor peptide PAP(248–286). *J Phys Chem B*. 2012;116:3650–3658.

Manuscript received Jan. 22, 2013, revision received Jun. 18, 2013, and final revision received Aug. 12, 2013.